

## OSTEOCHONDRAL INJURY DURING SIMULATED DROP LANDING COMPRESSION: PRE AND POST IMPACT MICRO-COMPUTED TOMOGRAPHY

Fatemeh Malekipour<sup>1</sup>, Denny Oetomo<sup>1</sup> and Peter Vee Sin Lee<sup>1</sup>

Department of Mechanical Engineering, University of Melbourne, Melbourne<sup>1</sup>

The purpose of this study was to investigate osteochondral injuries due to impact load. Average nominal strain of  $34\% \pm 5\%$  was applied to equine osteochondral plugs. The deformation of cartilage and bone on one plane was measured using real-time imaging during the impact. High resolution micro-computed tomography prior to and following the loading was used to investigate the extent of the damage to the specimens. The average peak strain in bone and cartilage was  $0.11 \pm 0.01$  and  $0.20 \pm 0.08$ , respectively. Micro-fractures were found in the  $\mu$ CT images in the subchondral bone, ranging from  $200\mu\text{m}$  to  $30\mu\text{m}$  wide. The 3D images of micro-fractures, obtained here, can be used for future studies of bone remodeling as a result of such impact-induced damages. The strain in the bone was significantly large indicating the ability of bone to absorb the impact energy.

**KEY WORDS:** Trauma, subchondral bone, deformation, real-time imaging,  $\mu$ CT.

**INTRODUCTION:** Impact-induced trauma to the knee joint is a key factor leading to post traumatic knee osteoarthritis. Such injuries are highly common in sports activities, especially during drop landing which can deliver around 35MPa of contact pressure to the joints' surface (Meyer, Baumer, Slade, Smith & Haut, 2008) at high rates. The injuries caused by such impact loads are usually in the form of articular cartilage (AC) fissures and subchondral bone (SB) micro-fractures (Vener, Thompson, Lewis & Oegema, 1992). Previous studies have used the whole joint either in-vivo or in-vitro to simulate such injuries (Borrelli, Torzilli, Grigiene & Helfet, 1997). Others also used osteochondral explants to study the injury as it provides a more controlled experimental condition (Jeffrey & Aspden, 2006; Yeow, Lau, Lee & Goh, 2009). However, most explants studies did not consider the underlying bone, focusing instead on the AC; the underlying bone in these specimens is usually buried in the cement. However, in the physiological conditions, the underlying bone could play a significant role in absorbing the impact energy and protect the AC from damage (Radin & Paul, 1971). Burgin et al. (Burgin & Aspden, 2008) measured the effective modulus of the combine bone and cartilage by varying the thickness of bone under impact load. They found that by decreasing the thickness of the underlying bone, the effective combined modulus of the bone and AC decreased as expected. However, the study did not investigate the contribution of the bone and AC individually in absorbing the impact load and the types of bone and AC damages. In this study, osteochondral plugs, containing the full thickness of AC and its underlying bone (1mm), was impacted to simulate the loading conditions similar to that of drop landing. Real-time imaging was used to measure the 2D deformation of AC and bone during loading. We hypothesized a large strain in SB and therefore a high ability of the underlying bone to absorb the impact energy.

**METHODS:** Five osteochondral plugs of size 9mm in diameter were extracted from fresh frozen tibial plateau of one mature (four years old) racehorse using a core drill. Water was used for irrigating the specimens while coring. The horse joint was chosen as there was evidence that the cartilage and subchondral plate thickness were similar to that of human joints (Frisbie, Cross, & McIlwraith, 2006). The plugs were subsequently fixed in dental cement leaving the full thickness of AC and 1mm of SB out of the cement. The embedded plugs were then cut vertically at one side using a diamond saw such that a smooth surface containing cartilage and bone was achieved. The created flat plane was stained by graphite particles prior to impact tests and exposed to the lens of a stereomicroscope (SZX7, Olympus, Japan) which was placed horizontally in front of the specimens. A level gauge was used to adjust the microscope to be perpendicular to the stained plane of the specimen. A

digital high speed camera (MotionPro, Y3, 1280x1024, 1000fps) was mounted to the microscope to capture real-time images of the specimen during loading. Controlled displacement was applied using a servo hydraulic mechanical testing machine (Instron, 8874, UK) to each specimen using a half sine waveform with frequency of 10 Hz. A fixture was designed and built to place the specimen in the testing machine. A cylindrical indenter of size 20 mm diameter was built to apply the compression to specimen surface. Prior to compression, thickness of each specimen was measured optically using the above mentioned imaging set-up. Based on the measured thickness, the displacement required to create a 30% strain was calculated and used for the impact test. The 30% strain was selected such that surface pressures of 35MPa, similar to that reported in drop landing scenarios (Meyer et al, 2008), could be generated with the specimens tested. A preload of 10N was applied prior to the impact test. Specimens were immersed in PBS (phosphate buffered saline) for one hour before testing. Prior to and following the loading, all specimens were scanned using a  $\mu$ CT scanner at resolution of 9  $\mu$ m (Skyscan-1076, Aartselaar, Belgium). In order to eliminate the ring artefacts typically found in  $\mu$ CT images, each specimen was placed in the  $\mu$ CT scanner's specimen holder with the aid of foam moulds at the exact same position before and after impact. The specimens were kept moist with PBS soaked gaze during testing. The acquired real-time images were processed later in Motion Studio software (IDT inc.) to obtain the deformation of the AC and SB at each time frame. The planar strain of AC and SB was calculated by dividing the calculated deformation to the original sets of thickness of AC and SB obtained from images before loading. In addition, nominal strain and stress were calculated using the collected load and displacement data from MTS by dividing the measured displacement and load by the initial thickness and surface area of the specimen. The surface area was obtained from pre-impact  $\mu$ CT images. Specimen modulus was calculated by dividing the stress into the strain at each time frame. Visual examination of  $\mu$ CT scanned images was performed to find the created damages. 3D reconstruction of the damages was achieved by segmenting the AC and SB in Skyscan software and to measure the size of the gaps and the width of the cracks.

**RESULTS:** The average peak stress and strains of AC and bone are listed in Table 1. Visual examination of the articular surface showed surface fissures in all specimens. The post-impact  $\mu$ CT images revealed oblique fissures which extended to the superficial layer. Fig.1a illustrates the 3D reconstructed images showing AC fissures from a specimen after impact. Gross fractures with associated step-off displacements were detected in the zone of calcified cartilage in three of five specimens (Figure 1b). The average failure stress for the three specimens was  $31.1 \pm 8.8$  MPa.

**Table 1: Average values and standard deviation of peak nominal strain, peak stress, peak modulus for combination of cartilage and bone, peak planar AC strain and SB strain.**

Mechanical parameter	Avg. $\pm$ SD
Nominal strain	0.34 $\pm$ 0.05
Stress (MPa)	24.56 $\pm$ 10.42
E (MPa)	77.11 $\pm$ 34.05
AC planar strain	0.20 $\pm$ 0.08
SB planar strain	0.11 $\pm$ 0.01

The bone damages were observed mostly at the boundary of the specimens. Visual examination of the three-dimensional geometries from  $\mu$ CT also showed that micro-fractures happened in the areas where the SB was raised into the calcified cartilage zone. Micro-cracks of size less than 30  $\mu$ m were observed around the fractures. In one specimen, occult cracks were found in the zone of calcified cartilage. In other specimens there were many micro-cracks in the bone which was revealed to be pre-existing when compared to the pre-impact  $\mu$ CT images. The gross fractures were mostly extended oblique down to the bone whereas the occult micro-crack was vertically extended. The width of the micro-fractures varied from 80-200  $\mu$ m. However, micro-cracks of approximate size 30  $\mu$ m were also

observed extending from the calcified region down to the trabecular bone in the inner ring of one specimen, which is presented in Figure 1c, d.

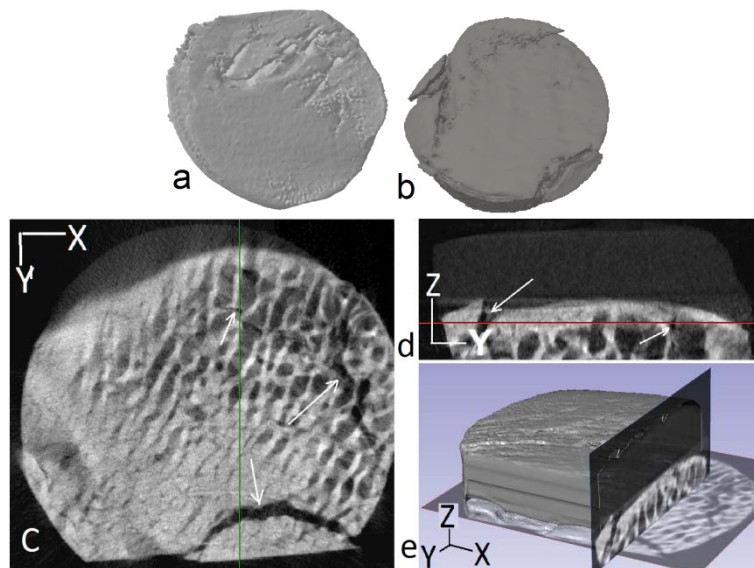


**Figure 1: 3D reconstructed image, a) AC and b) SB showing AC surface fissures and SB microfractures, c) Transverse and d) sagittal post-impact  $\mu$ CT slices from e) fracture sites.**

An example of strain curve versus loading time is presented in Figure 2 for no-failure (a) and with-failure (b) experiments. The AC strain was approximately twice the SB strain in no-failure tests whereas a drop of AC strain was seen in the with-failure experiments.

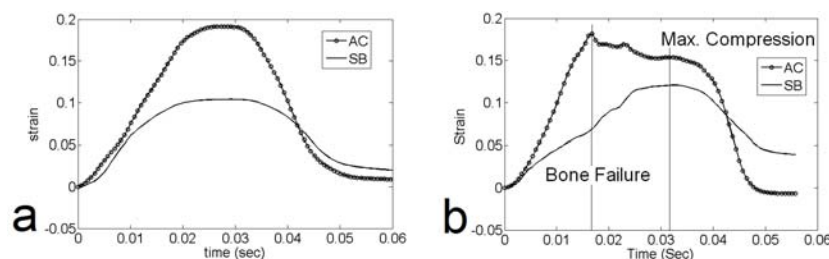


**Figure 2: AC and SB planar strain versus loading time, a) no-failure and b) with-failure (b).**

**DISCUSSION:** The purpose of this study was to simulate the injury to the cartilage and bone during impact load (drop landing). Unlike most of osteochondral studies, we chose to expose the underlying bone to the applied strain so that a situation more similar to in-vivo boundary conditions can be achieved for cartilage. Based on our results, the ratio of SB/AC strain was approximately 1/2. Assuming a minimum approximate ratio of 400/40 for SB/AC stiffness (Finlay & Repo, 1978), a value of 2.5 ( $10 \times 1/2^2$ ) for the ratio of energy absorbed per volume of bone to cartilage can be estimated. Thus, the high value of the bone strain confirmed our hypothesis indicating that bone absorbs a relatively high amount of impact energy. Moreover, if there is a failure in the bone, more energy would be absorbed in the form of plastic deformation which can be protective to cartilage by reducing the deformation.

With the aid of the  $\mu$ CT, we were able to detect impact-induced cracks of width size 30  $\mu$ m in bone as well as 3D fissures of the cartilage. The oblique surface fissures of the cartilage and vertical shape and size of bone cracks are in agreement with previous studies that have used entire joints to induce impact injuries (Vener et al., 1992; Meyer et al., 2008) and also cartilage explants (Jeffrey et al., 2006). Apart from the fractures of the outer ring of the specimens, no more occult cracks were found inside the specimens despite the relatively high planar strain that was created in the SB ( $11 \pm 1.0\%$ ). The comparison of post-impact images with corresponding pre-impact images assured us that the cracks were created because of the impact load. There were several cases where the detected cracks were thought to be found, however, more investigation revealed the exact same ones in the pre-

impact  $\mu$ CT images. The bone micro-fractures at the outer ring of the plugs seem most likely to be caused by the lack of support from neighbor trabeculae in an unconfined compression. However, more investigations of the 3D geometry of the specimens showed that almost all of the fractures have occurred in the areas where SB was raised to the calcified cartilage creating a site of stress concentration. Computational studies using the real geometries from  $\mu$ CT images in this study can help understand the mechanical factors of the fractures in future studies. Conventional methods such as histology may not be accurate enough due to artifacts during preparation of the sections. In addition, it is impossible using such methods to distinguish the cracks created because of the impact from pre-existing cracks. Bulk staining is another method that researchers have used to visualize the micro-cracks in the bone, but 3D geometry is not possible with this method.

There is strong evidence that bone remodeling triggered by such micro-cracks may be the reason for post traumatic osteoarthritis in the joint (Burr & Radin, 2003). The method we used to obtain the width and length of the fractures and cracks can provide detailed and specimen-specific information to investigate bone remodeling. Moreover, a molecular interaction is believed to exist at the interface of AC and SB (Lories & Luyten, 2010). Such interaction can be highly dependent on the pressure distribution at the interface. The 3D geometry of the damages from our results can be employed to model the alterations that impact-induced injuries bring about to either the overlying cartilage mechanical behavior or the load distribution at the interface of bone and cartilage.

**CONCLUSION:** The mechanical behaviour of AC-on-SB specimens under axial compression similar to drop landing was investigated by measuring the strain of the cartilage and bone separately. Based on our results the AC strain drops following the bone failure so we can conclude that SB protects articular cartilage by limiting the amount of deformation absorbed by AC. The impact-induced micro-cracks were measured and visualised three dimensionally using  $\mu$ CT scanning. We also suggest that if the mechanical behavior and extent of injury to the joint is going to be investigated, including the underlying bone in osteochondral specimens is necessary as it affects the overlying cartilage deformation significantly.

#### REFERENCES:

- Borrelli Jr, J., Torzilli, P., Grigienė, R. & Helfet, D. (1997). Effect of impact load on articular cartilage: development of an intra-articular fracture model. *Journal of orthopaedic trauma*, 11, 319-326.
- Burgin, L.V., Aspden, R.M. (2008), Impact testing to determine the mechanical properties of articular cartilage in isolation and on bone. *Journal of Materials Science*, 19, 703-711.
- Burr, D. & Radin, E. (2003). Microfractures and microcracks in subchondral bone: are they relevant to osteoarthritis? *Rheumatic Disease Clinics of North America*, 29, 675-685.
- Finlay, J. & Repo, R. (1978). Cartilage impact in vitro: effect of bone and cement. *Journal of Biomechanics*, 11, 379-385.
- Frisbie, D., Cross, M. & McIlwraith, C. (2006). A comparative study of articular cartilage thickness in the stifle of animal species used in human pre-clinical studies compared to articular cartilage thickness in the human knee. *Veterinary and comparative orthopaedics and traumatology*, 19, 142-146.
- Jeffrey, J. & Aspden, R. (2006). The biophysical effects of a single impact load on human and bovine articular cartilage. *Proceedings of the Institution of Mechanical Engineers, Part H: Journal of Engineering in Medicine*, 220, 677-686.
- Lories, R. & Luyten, F. (2010). The bone--cartilage unit in osteoarthritis. *Nature Reviews Rheumatology*, 7, 43-49.
- Meyer, E., Baumer, T., Slade, J., Smith, W. & Haut, R. (2008). Tibiofemoral contact pressures and osteochondral microtrauma during anterior cruciate ligament rupture due to excessive compressive loading and internal torque of the human knee. *The American Journal of Sports Medicine*, 36, 1966-1977.
- Radin, E., Paul, I. (1971). Importance of bone in sparing articular cartilage from impact. *Clinical orthopaedics and related research*, 78, 342-345.
- Vener, M., Thompson Jr, R., Lewis Jr, J. & Oegema Jr, (1992). T. Subchondral damage after acute transarticular loading: an in vitro model of joint injury. *Journal of orthopaedic research*, 10, 759-765.

Yeow, C., Lau, S., Lee, P. & Goh, J. (2009). Damage and degenerative changes in menisci-covered and exposed tibial osteochondral regions after simulated landing impact compression-a porcine study. *Journal of Orthopaedic Research*, 27, 1100-1108.